Geol. Mag. **155** (*6*), *2018, pp. 1230–1246.* © *Cambridge University Press 2017*
doi:10.1017/S0016756817000140

New constraints from zircon, monazite and uraninite dating on the commencement of sedimentation in the Cuddapah basin, India

DEBIDARSANI SAHOO*, KAMAL LOCHAN PRUSETH*†, DEWASHISH UPADHYAY*, SAMEER RANJAN*, DIPAK C. PAL‡, RAHUL BANERJEE§ & SHEKHAR GUPTA§

*Department of Geology and Geophysics, Indian Institute of Technology, Kharagpur–721302, India
‡Department of Geological Sciences, Jadavpur University, Kolkata–700032, India
§Atomic Mineral Directorate for Exploration and Research, Department of Atomic Energy, India

(*Received* 6 November 2016; *accepted* 7 February 2017; *first published online* 4 April 2017)

Abstract – The Cuddapah basin in southern India, consisting of the Palnad, Srisailam, Kurnool and Papaghni sub-basins, contains unmetamorphosed and undeformed sediments deposited during a long span of time in the Proterozoic. In the absence of robust age constraints, there is considerable confusion regarding the relative timing of sedimentation in these sub-basins. In this study, U–Pb isotopic dating of zircon and U–Th–Pb_{total} dating of monazite and uraninite from the gritty quartzite that supposedly belongs to the formation Banganapalle Quartzite have been used to constrain the beginning of sedimentation in the Palnad sub-basin. Magmatic and detrital zircons recording an age of 2.53 Ga indicate that the sediments were derived from the granitic basement or similar sources and were deposited after 2.53 Ga. Hydrothermally altered zircons both in the basement and the cover provide concordant ages of 2.32 and 2.12 Ga and date two major hydrothermal events. Thus, the gritty quartzite must have been deposited sometime between 2.53 and 2.12 Ga and represents the earliest sediments in the Cuddapah basin. Monazite and uraninite give a wide spectrum of ages between 2.5 Ga and 150 Ma, which indicates several pulses of hydrothermal activity over a considerable time span, both in the basement granite and the overlying quartzite. The new age constraints suggest that the gritty quartzite may be stratigraphically equivalent to the Gulcheru Quartzite that is the oldest unit in the Cuddapah basin, and that a sedimentary/erosional hiatus exists above it.

Keywords: Banganapalle, Purana basins, LA–ICPMS zircon dating, chemical dating, siliceous stromatolite.

1. Introduction

The Proterozoic basins of India, also known as the Purana basins, comprise vast thicknesses (e.g. Cuddapah basin: area 44 500 km^2, thickness 10–12 km (Nagaraja Rao *et al.* 1987); Vindhyan basin: area 162 000 km^2, thickness ~5 km (Prasad & Rao, 2006); Chhattishgarh basin: area 33 000 km^2, thickness ~2.3 km (Chakraborty *et al.* 2012)) of undeformed and unmetamorphosed sediments. The crescent-shaped Cuddapah basin in southern India is one such Purana basin, well known for its thick sequence of Palaeoproterozoic and Mesoproterozoic sedimentary successions (Fig. 1). The basin is subdivided into four sub-basins: the Papaghni, Kurnool, Srisailam and Palnad (Nagaraja Rao *et al.* 1987). The Nallamalai schist belt had earlier been thought to be the deformed eastern part of the Cuddapah sequence affected by Proterozoic tectono-metamorphic events (King, 1872; Narayanswami, 1966; Meijerink, Rao & Rupke, 1984; Lakshminarayana, Bhattacharjee & Ramanaidu, 2001). Some recent studies (e.g. Saha & Chakraborty, 2003; Saha, Chakraborti & Tripathy, 2010), however, consider the schist belt to be a separate crustal entity juxtaposed against the Cuddapah basin rocks along a major N–S thrust. The Kurnool and Palnad sub-basins were earlier stratigraphically correlated with the Vindhyan and Chhattisgarh basins (Medlicott & Blanford, 1879; Raha, 1987; Chaudhuri *et al.* 2002), which were assigned a Neoproterozoic age (Azmi, 1998; De, 2003, 2006; Azmi *et al.* 2006, 2008; Joshi, Azmi & Srivastava, 2006; Kumar & Pandey, 2008). However, the oldest sediments in the Vindhyan basin have recently been shown to be Palaeo- to Mesoproterozoic in age (e.g. 1721–1600 Ma (Rasmussen *et al.* 2002; Ray *et al.* 2002; Ray, Veizer & Davis, 2003; Sarangi, Gopalan & Kumar, 2004; Bengtson *et al.* 2009)) and those in the Chhattisgarh basin to be ~1400 Ma (Bickford *et al.* 2011). The depositional age of the Kurnool Group of sediments in the Cuddapah basin is not yet adequately constrained.

Sharma & Shukla (2012) have argued for a Neoproterozoic age of the Kurnool basin, based on the occurrence of helically coiled Ediacaran *Obruchevella* species in the Owk Shale and burrow structures in the underlying Narji Limestone. However, the presence of sedimentary carbonate xenoliths, purportedly belonging to the Kurnool or its equivalent Bhima

†Author for correspondence: pruseth@gg.iitkgp.ernet.in

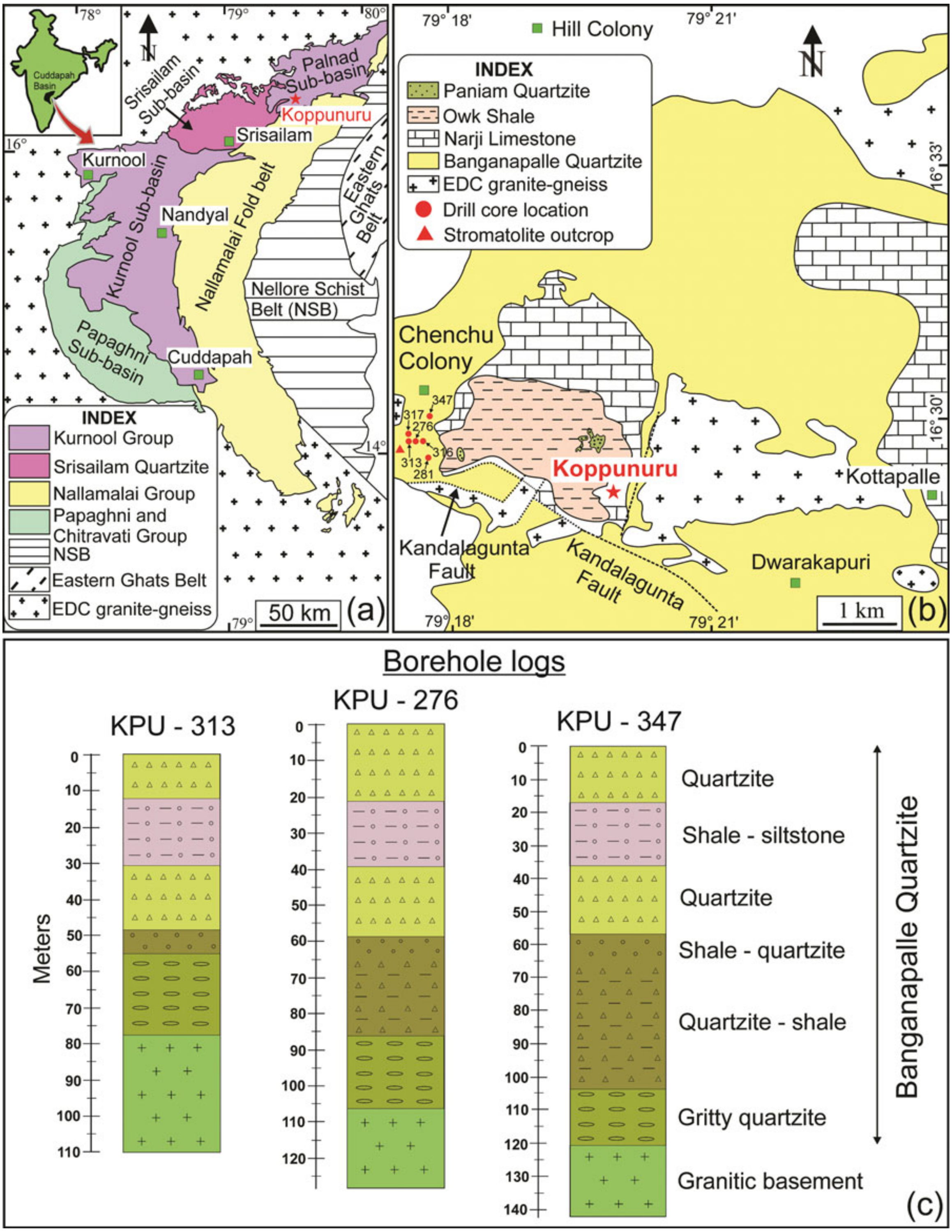

Figure 1. (Colour online) Geological map of the study area and sample locations. (a) The Cuddapah basin in southern India with its sub-basins demarcated (after Nagaraja Rao *et al.* 1987); (b) sample drill core sites shown on the geological map of the Koppunuru area in the Palnad sub-basin (after Jeyagopal *et al.* 2011); (c) three selected borehole logs showing variable thickness and unevenness of the gritty quartzite.

basin (A. Dongre *et al.* unpub. abstract, 2007; Dongre, Chalapathi Rao & Kamde, 2008; Chalapathi Rao *et al.* 2010) in the Siddanpalli and Raichur kimberlites, dated at ∼1090 Ma (Kumar, Heaman & Manikeyamba, 2007), suggests that the sediments were deposited before 1090 Ma. In contrast, the occurrence of diamonds inferred to be derived from the 1140–1105 Ma (Crawford & Compston, 1973; Osborne *et al.* 2011) Wajrakarur kimberlite pipes (Krishnan, 1964; Nagaraja Rao *et al.* 1987; Chaudhuri *et al.* 1999) in the Banganapalle Conglomerate, which forms the base of the Kurnool Group, indicates that the sediments are younger than 1105 Ma, in consonance with the observation of Sharma & Shukla (2012).

https://doi.org/10.1017/S0016756817000140 Published online by Cambridge University Press

Bickford *et al.* (2013) have dated detrital zircons from an apparent felsic tuff bed (Saha & Tripathy, 2012) *c.* 110–200 m above the base of the Kurnool rocks, which yielded ages similar to that of the ~2.5 Ga basement. Collins *et al.* (2015) obtained youngest detrital zircon ages of 2516 ± 16 Ma from the Banganapalle Quartzite, which again represent the age of the basement. Thus the timing of initiation of sedimentation in the Kurnool basin still remains unconstrained. A single age of 913 ± 11 Ma (Collins *et al.* 2015) from the Paniam Quartzite in the upper Kurnool succession suggests a much younger age for the cessation of sedimentation.

In this contribution, we have dated (1) magmatic zircon in the basement granites, (2) detrital zircon in the overlying gritty quartzite and (3) hydrothermally altered zircon from the basement granite as well as the gritty quartzite, using U–Pb isotopes on a laser ablation inductively coupled plasma mass spectrometer (LA-ICPMS). Together with the results of chemical Th–U–Pb_{total} EPMA (electron probe micro analysis) dating of uraninite from the gritty quartzite and hydrothermally altered monazite in the basement granite, we constrain the timing of initiation of sedimentation in the Palnad sub-basin. The gritty quartzite hosts uraninite mineralization. We observe that occasional veins of brannerite cross-cut the uraninite occurrences and that uraninite has been partially replaced by later coffinite. The repeated remobilization of U in the quartzite reflects episodic hydrothermal activity that also affected the granitic basement.

2. Geological background and sample

Samples were collected from the Palnad sub-basin, situated in the NE part of the Cuddapah basin. It is considered to be equivalent to the Kurnool Group of rocks exposed in the W part of the same basin (Fig. 1a). Stratigraphically, the Kurnool Group is younger than the Cuddapah Supergroup and lies above it with an angular unconformity (Table 1). Our study area around Koppunuru (16° 29′ 19″ N, 79° 19′ 50″ E) is located near the western margin of the Palnad sub-basin, where the Banganapalle Quartzite, the lowermost formation of the Kurnool Group, directly overlies the basement granites and gneisses of the Eastern Dharwar Craton (EDC), and the upper two formations, the Koilkuntala Limestone and the Nandyal Shale, are absent. The geological map of the region is shown in Figure 1b.

Because of the horizontal to sub-horizontal disposition, the full thicknesses of the formations are not exposed. The samples from the Banganapalle Quartzite are from the drill core repository of the Atomic Mineral Directorate (AMD), Government of India. The drill core sites are indicated in Figure 1b. Logs of three selected drill cores are provided in Figure 1c. The lowermost unit in the drill cores is the gritty quartzite, which is followed by a quartzite–shale unit, a lower quartzite, a shale–siltstone and an upper quartzite. The quartzite–shale unit is more shale-rich at the top and has variable thickness from one borehole to another. The variable thickness of the uppermost quartzite can be ascribed to differential surface erosion. Surface samples of quartzite were also collected from near Chenchu Colony (16° 29′ 45″ N, 79° 17′ 20″ E) and Dwarakapuri (16° 28′ 05″ N, 79° 21′ 05″ E). One sample of basement granite showing high radioactivity was collected from the Hill Colony site (16° 34′ 40″ N, 79° 19′ 19″ E) situated at the margin of the basin.

3. Methodology and analytical conditions

3.a. EPMA chemical dating of monazite and uraninite

Monazite from the granite and uraninite from the quartzite were dated by measuring their U, Th and Pb concentrations using a Cameca SX-100 Electron Probe Micro Analyzer (EPMA) at the Department of Geology and Geophysics, Indian Institute of Technology (IIT), Kharagpur. This method has the advantage of extracting chemical analyses from small domains of a mineral grain because of the small probe beam size (~1 μm), thus providing highly spatially resolved age information. Both monazite and uraninite incorporate negligible Pb at the time of their formation, and the radiogenic Pb accumulated in them is a function of their U and Th concentrations, and the time elapsed since their formation. Fluid-induced dissolution–reprecipitation processes may re-equilibrate and reset the U–Th–Pb decay system in pre-existing grains or may precipitate new grains as well as overgrowths on older ones, thus preserving a record of the geological events affecting the rocks. These individual zones can normally be identified by backscattered electron (BSE) imaging. The relation between Pb concentration and age is given by

$$\mathrm{Pb} = \frac{\mathrm{Th}}{232} \times \left(e^{\lambda_{232}t} - 1\right) \times 208 + \frac{U}{238.03} \times \left(e^{\lambda_{238}t} - 1\right) \times 0.9928 \times 206 + \frac{U}{238.03} \times \left(e^{\lambda_{235}t} - 1\right) \times 0.0072 \times 207$$

in which λ_{232}, λ_{238} and λ_{235} are the decay constants for ^{232}Th, ^{238}U and ^{235}U, respectively. Present-day relative proportions of ^{238}U and ^{235}U in natural uranium are respectively 0.9928 and 0.0072. The decay of ^{232}Th results in ^{208}Pb, and ^{238}U and ^{235}U respectively decay to ^{206}Pb and ^{207}Pb.

For the EPMA analyses of monazite and uraninite, typical operating conditions were 20 kV accelerating voltage, 150 nA beam current and 1 μm beam diameter. The Kα lines of Si and Al and the Lα line of Y were measured on TAP, Ca–Kα, Th–Mα and U–Mβ were measured on PET, Fe–Kα, Pr–Lβ, Nd–Lβ, Sm–Lα, Gd–Lβ, Dy–Lα and Ho–Lβ were determined on LIF, whereas P–Kα, Zr–Lα, La–Lα, Ce–Lα and Pb–Mα were measured on a large PET crystal. The elements Si, Al, Fe and P were counted for 10 s on the

Table 1. Lithostratigraphic succession of the Cuddapah Supergroup and Kurnool Group (after Nagaraja Rao *et al.* 1987; Tripathy & Saha, 2013)

Supergroup	Group	Formation	Intrusives
	Kurnool Group	Nandyal Shale	
		Koilkuntala Limestone	
		Paniam Quartzite	
		Owk Shale	
		Narji Limestone	
		Banganapalle Quartzite	
		Unconformity	
Upper Cuddapah Supergroup		Srisailam Quartzite	Kimberlite pipes (*c.* 1090 Ma)
		Unconformity	
		Cumbum Shale	Chelima lamproite (*c.* 1400 Ma)
	Nallamalai Group	Bairenkonda Quartzite	
		Unconformity	
Lower Cuddapah Supergroup	**Chitravati Group**	Gandikota Quartzite	
		Tadpatri Shale	Mafic sills (*c.* 1800 Ma)
		Pulivendla Quartzite	
		Disconformity	
	Papaghni Group	Vempalle Limestone	
		Gulcheru Quartzite	
		Nonconformity	
	Peninsular Gneiss//Dharwar Schists		

peak. Similarly, Ca, La and Ce were measured for 20 s; Nd, Sm, Gd and Y for 40 s; Dy and Ho for 60 s; Th and U for 200 s; and Pb for 300 s. Respective background intensities were measured on both sides of the peak for half the peak times. The Pb–Mα line was corrected for overlap from the second- and third-order reflections of Y–Lγ whereas U–Mβ was corrected for interference from Th–Mγ, and Gd–Lβ was corrected for the interfering Ho–Lα. The elements Al, Th and U were calibrated on standards of their respective oxides and Fe on hematite. An apatite standard was used to calibrate Ca and P. All the rare earth elements (REE) were calibrated on standard REE glasses, Si on a Th-containing glass, Zr on zircon, Y on Yttrium Aluminum Garnet and Pb on pyromorphite. All standards were supplied by P&H Developments Ltd (UK).

3.b. LA-ICPMS U–Pb dating of zircon

Zircon grains from the basement granite were dated *in situ* in thin sections using a LA-ICPMS at the Department of Geology and Geophysics, IIT, Kharagpur. Cathodoluminescence (CL) and BSE images of the zircon grains obtained using a JEOL JSA 6490 Scanning Electron Microscope (SEM) were used as guides for spot selection. The U–Pb isotope measurements were done on a Thermo-Fisher Scientific ICAP-Q quadrupole ICPMS coupled to a New Wave 193 ArF Excimer laser ablation system. The laser was operated at 5 Hz repetition rate, 5 J cm^{-2} beam energy density and 25 μm spot size. The ICPMS was optimized for maximum sensitivity on Pb, Th and U using the NIST 612 reference glass. The oxide production rate monitored on ^{232}Th^{16}O was found to be <0.5 %. The analyses were performed in a time-resolved mode, with each analysis consisting of 30 s background measurement and 40 s peak signal measurement. External standardization was done by bracketing groups of ten unknowns with three measurements of the GJ-1 reference zircon (Jackson *et al.* 2004). The data were reduced offline using an in-house Excel© spreadsheet that corrects for instrumental and gas backgrounds, laser-induced elemental fractionation, and instrumental mass-bias and drift. The uncertainty on each analysis was estimated by quadratic addition of the 2SE (standard error) internal run statistics of each analysis and the 2σ of isotopic ratios measured in the bracketing GJ-1 reference zircon. To monitor precision and accuracy, the 91500 reference zircon (Wiedenbeck *et al.* 1995) was analysed ($n = 4$) as unknown. The ^{206}Pb/^{238}U (0.1789 ± 1.1 %, 2σ) and ^{207}Pb/^{206}P (0.0745 ± 0.33 %, 2σ) ratios measured for this zircon match published values within analytical errors. All uncertainties are reported at the 2σ level. The U contents were estimated relative to the GJ-1 reference zircon. Concordia diagrams and age probability/histogram plots were constructed using Isoplot 4.15 (Ludwig, 2003).

4. Results

4.a. Monazite ages

The U, Th and Pb concentrations along with the apparent spot ages from monazites in the basement granite are provided in the supplementary Table S1. Larger errors in some spot ages reflect their low Th and Pb concentrations. Therefore, while older ages with >10 % errors have been discarded, ages younger than 500 Ma with up to 15 % error have been considered, as these ages are fewer in number and have higher errors due to lower radiogenic Pb contents. The calculated ages span from 2958 to 243 Ma and define one major and several minor peaks in the age probability density plot (Fig. 2a). The majority of the ages define a peak at 2504 ± 19 Ma. The BSE images reveal the presence of two textural varieties of monazites: some grains are

https://doi.org/10.1017/S0016756817000140 Published online by Cambridge University Press

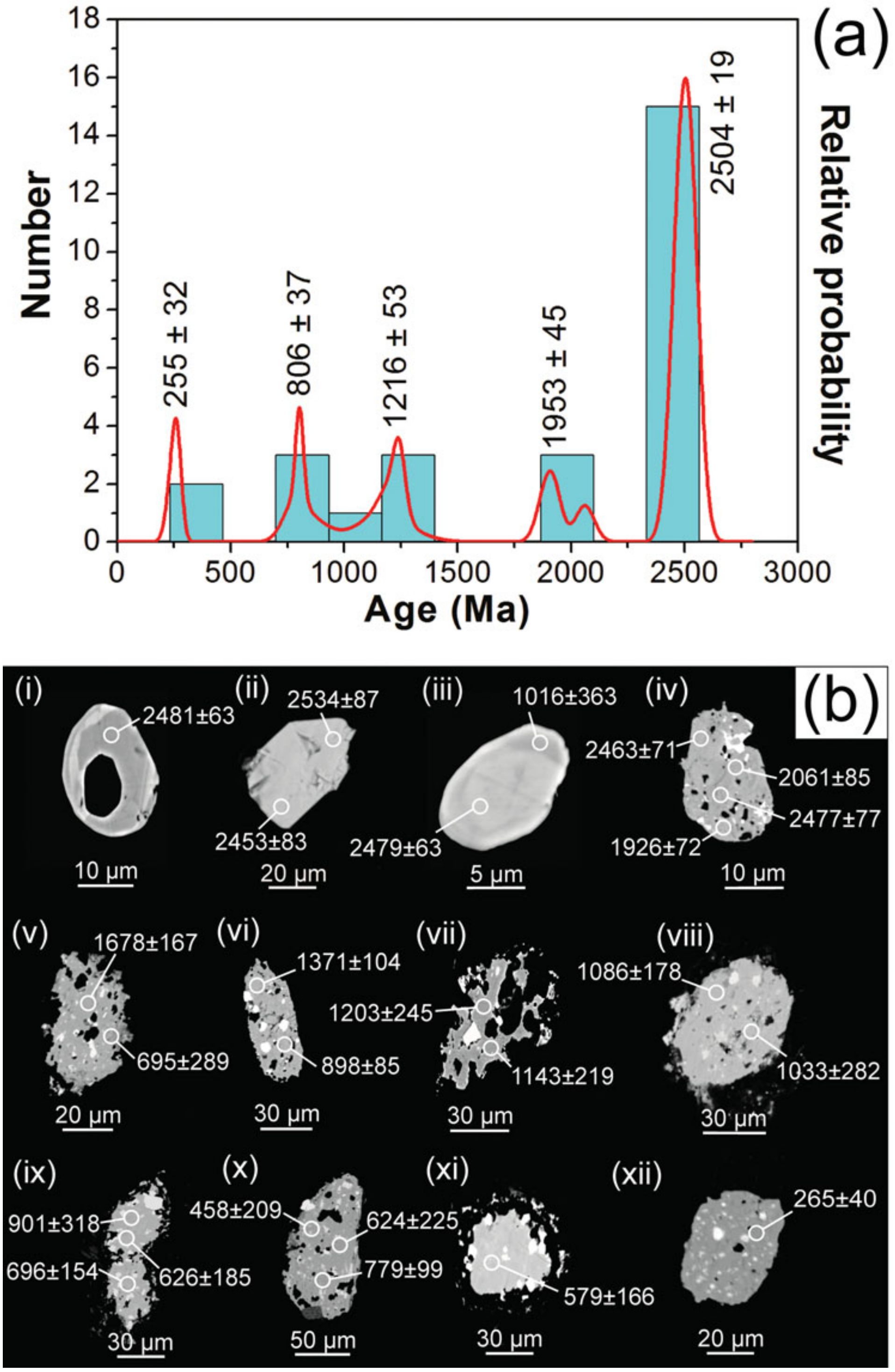

Figure 2. (Colour online) Monazite EPMA U–Th–Pb_{total} ages from the basement granite. (a) Probability density plot showing a prominent peak at the older age end and several smaller peaks at lower ages; (b) representative BSE images showing the analysed spots and the corresponding ages obtained. The monazite microtextures record intense hydrothermal alterations which give ages ranging over ~2500– 250 Ma.

relatively euhedral and preserve faint traces of oscillatory growth zones (e.g. Fig. 2b grains i, iii); others are micro-porous and characterized by sieve texture, irregular corroded boundaries and the presence of numerous inclusions of thorite and xenotime (Figs 2b, 3a–d). Such textures are usually produced by extensive fluid-induced alteration involving dissolution of U–Th–Y-rich monazite and precipitation of U–Th–Y-poor hydrothermal monazite (Table S1). Uranium being mobile was removed by the fluid, while Th and Y behaved as immobile elements precipitating as thorite and xenotime inclusions in micropores within monazite. The euhedral and unaltered monazite grains overwhelmingly give ages which define the ~2500 Ma

https://doi.org/10.1017/S0016756817000140 Published online by Cambridge University Press

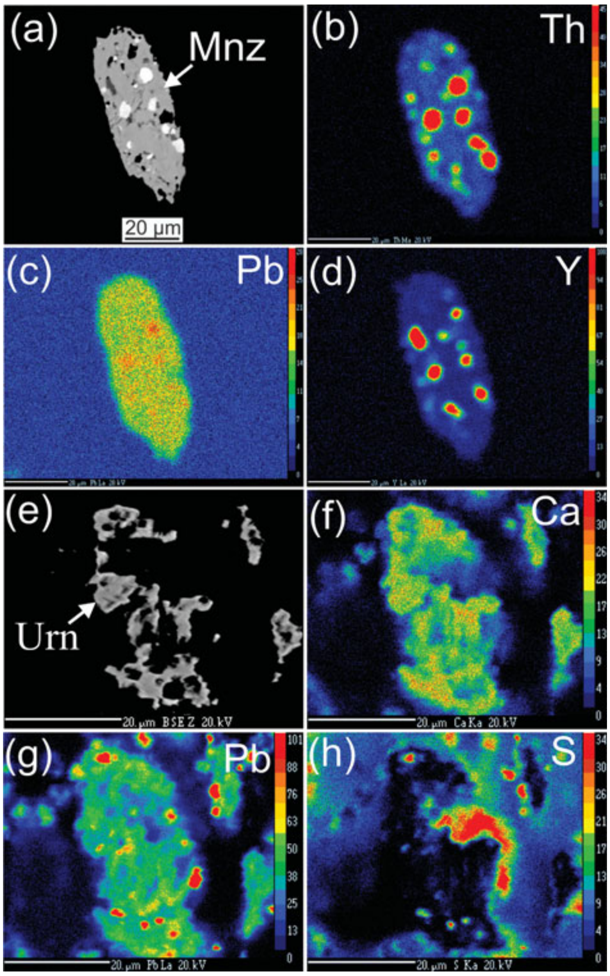

Figure 3. (Colour online) BSE image and X-ray element maps showing alteration of monazite in the basement granite (a–d) and uraninite in the Banganapalle Quartzite (e–h). In monazite, precipitation of thorite and xenotime is evident from the segregation of Th and Y, and Pb is uniformly distributed in the reprecipitated monazite. Fine granular nature of uraninite is evident from the Ca and Pb distribution patterns. Segregation of Pb-rich domains is seen within the uraninite, which may give rise to spurious age estimates. High S in a patch of carbonaceous matter (h) indicates derivation of S from organic matter for the formation of galena (spots with both high Pb and high S). Abbreviations: Mnz = monazite, Urn = uraninite.

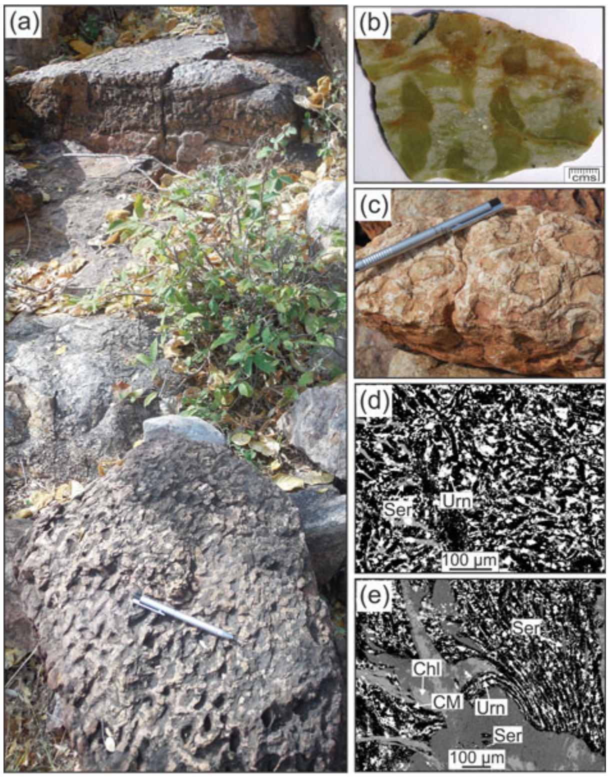

Figure 4. (Colour online) Stromatolitic structures in the Banganapalle Quartzite. (a) Columnar siliceous stromatolites with raised boundaries of resistant silica-cemented medium to fine sand; (b) unaltered siliceous stromatolite and thrombolite; (c) altered stromatolite resembling pebbles; (d) random precipitation of uraninite in carbonaceous-matter-rich masses, probably due to reduction of remobilized U in oxidizing fluids; (e) fragments of stromatolitic laminations of uraninite alternating with organic carbon-rich layers. Abbreviations: Chl = chlorite, CM = carbonaceous matter, Ser = sericite, Urn = uraninite.

population. This age is interpreted to date the emplacement of the granites. The hydrothermally altered monazites give a wide range of ages which define the minor peaks in the age probability density plot (Fig. 2a).

4.b. Uraninite ages

The Banganapalle Quartzite hosts siliceous stromatolites (Fig. 4a–c). Fine-grained uraninite mineralization is associated with sporadic occurrences of well-preserved microbial organic matter. Randomly oriented uraninite and sericite occur within masses of organic matter (Fig. 4d). However, domains preserving stromatolite-like laminations of alternate organic matter and fine-grained uraninite are sometimes encountered (Fig. 4e). Uraninite from the mineralized zones, associated with organic matter in the basal gritty quartzite of the Banganapalle Quartzite formation, was dated using the EPMA.

Because of high concentrations of U and Pb, the uraninite analyses have smaller analytical uncertainties even for relatively younger grains (see supplementary Table S2). However, BSE images and X-ray element mapping reveal microtextures indicating fluid-induced alteration in the uraninites (Fig. 3e–h). In BSE images, uraninite appears as irregular patches, whereas in the Ca and Pb X-ray maps a granular nature is evident, implying that the apparently irregular patches are most likely accumulations of Ca-bearing colloidal precipitates of uraninite. The segregation of Pb to form galena is evident from the correspondence of some high-Pb spots with high-S spots (Fig. 3g and h). Some high-S patches (Fig. 3h) are associated with organic matter, suggesting that the S in the galena was remobilized from the organic matter. The EPMA dating of uraninite is plagued by the following complications: (1) spuriously high Pb concentrations in some spots, due to mixed analyses of galena finely intergrown with the uraninite, resulting in ages that are too old and

https://doi.org/10.1017/S0016756817000140 Published online by Cambridge University Press

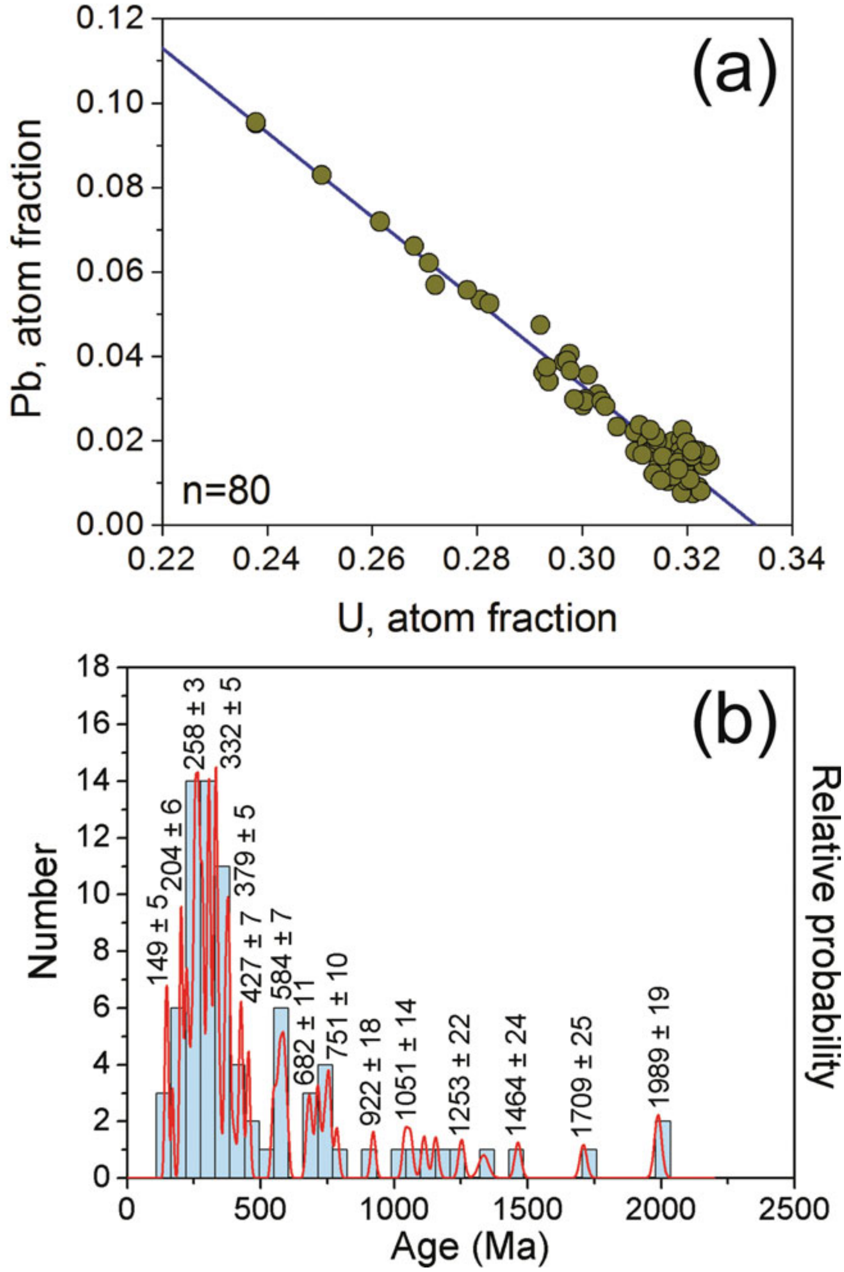

Figure 5. (Colour online) Uraninite EPMA chemical ages from the Banganapalle Quartzite. (a) Pb atom fractions plotted against U atom fractions for the uraninite analyses considered for age estimation plot along a line of –1 slope indicating negligible extraneous Pb; (b) probability density plot showing the effect of younger hydrothermal dissolution–reprecipitation of uraninite reflected in the erasure of the older age records.

of doubtful geological significance, (2) low analytical precision on some spots due to mixed analyses of fine sericite associated or intergrown with the uraninite and (3) concentrations below the detection limit of Pb in some uraninites, due to recent Pb loss. Given these analytical complications, only those analyses that plot along a line corresponding to a slope of –1 in the Pb vs U bivariate plot (Fig. 5a) were considered for the age calculations. This is because for every atom of U that undergoes radioactive decay, exactly one atom of radiogenic Pb will be added. The uraninite spot ages range from 144 to 1992 Ma and define a composite broad peak with an age maximum at ∼258 Ma (Fig. 5b).

4.c. Zircon ages

Zircon grains in the basement granite and the overlying gritty quartzite show evidence of extensive fluid-induced alteration via dissolution–reprecipitation processes. In the basement granite, the U- and Th-rich, possibly metamict, oscillatory growth zones have been selectively replaced by relatively U-poor and Ca–Si–LREE (light REE)-rich hydrothermal zircon (Fig. 6a, b). Similar selective alteration of U- and Th-rich growth zones is also seen in zircons from the gritty quartzite, with the metamict zones having been completely removed in some grains, preserving only the skeletal more resistant parts (Fig. 6c, d). The

https://doi.org/10.1017/S0016756817000140 Published online by Cambridge University Press

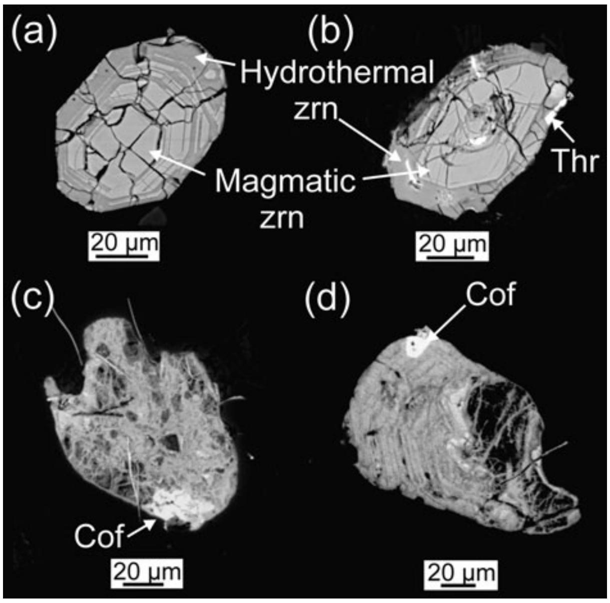

Figure 6. Representative BSE images showing extensive fluid-induced alteration of zircon. Original magmatic zoning patterns are preserved in the basement granite (a, b), whereas much more intense alteration giving rise to skeletal zircons is evident in the Banganapalle Quartzite (c, d). Abbreviations: Cof = coffinite, Thr = thorite, Zrn = zircon.

hydrothermally altered zircon and the unaltered zircon are geochemically distinct (Fig. 7; Table 2). The altered zircons have lower oxide totals (~83–90 wt %) in their EPMA analyses and have higher non-formula cations (e.g. Ca, Al and Fe). They are highly REE-enriched, particularly in the LREE (also reflected in the higher La/Y values) relative to the unaltered or weakly altered zircons, which have REE concentrations comparable to that of typical magmatic zircons. The Th/U ratios in the unaltered zircons vary in a narrow range of 0.49–0.55, whereas those in the altered zircons are more variable, having values between 0.38 and 7.14. Representative BSE and CL images with the LA-ICPMS spot ages are shown in Figure 8. The U–Pb isotope data (Table 3; Fig. 9) reveal the presence of both concordant and discordant age domains. The oscillatory-zoned unaltered parts of the grains in both the granite and the gritty quartzite yield concordant age populations, at 2538 ± 33 Ma and 2528 ± 8 Ma, respectively. Zircons from the granite additionally yield two concordant spot ages at 2127 ± 39 Ma. A similar concordant age of 2112 ± 43 Ma is obtained from one zircon grain in the quartzite. These ages are from domains which are patchily zoned or have ghost-like or bleached relic zoning typically seen in recrystallized zircons (Geisler, Schaltegger & Tomaschek, 2007; Harley, Kelly & Möller, 2007). An intermediate concordant age of 2325 ± 40 Ma is obtained in both the granite and the gritty quartzite. The discordant data points define discordias that indicate Pb loss from both the 2530 Ma and 2120 Ma zircons at ~90 Ma.

5. Discussion

5.a. The age of sedimentation of the gritty quartzite

The 2.53 Ga age from magmatic zircons in the granite dates the emplacement of the granitic basement of the Palnad sub-basin. The overlying gritty quartzite contains detrital zircons which overwhelmingly give 2.53 Ga ages, identical to those from the granites. This indicates that the sediments comprising the gritty quartzite were largely derived from the granitic basement or similar sources. It also indicates that the succession was deposited after 2.53 Ga.

The zircon, monazite and uraninite in both the basement granite and the gritty quartzite show evidence of intense hydrothermal alteration. Both rock units were affected by several pulses of hydrothermal activity, with the minerals in the gritty quartzite having been more intensely altered than those in the basement granite, possibly due to the greater permeability of the quartzites for the hydrothermal fluids. Several of the zircon grains in the quartzite have a delicate sieve-like porous structure. The alteration/dissolution that produced these microtextures must have happened *in situ* after the deposition of the quartzite since both the basement and the overlying quartzites were affected with similar alteration features and because grains with such delicate sieve-like structures are unlikely to survive sedimentary transport. The unaltered domains in zircon have Th/U values close to 0.5, which is characteristic of magmatic zircons (Hoskin & Schaltegger, 2003), whereas the altered zircons have widely variable Th/U ratios having values between 0.38 and 7.14. If non-fractionation of U and Th during zircon crystallization is assumed, the metamictized zones should also have had similar Th/U ratios prior to alteration. This would mean that the variable Th/U ratios in the altered zircon can be ascribed to preferential loss of U, causing them to plot above the line shown in Figure 7b, which is corroborated by the precipitation of thorite in the vicinity of zircon (e.g. Fig. 6b). Submicroscopic thorite grains could be contributing to the inhomogeneous distribution of Th in zircon as evident in the LA-ICPMS analyses. The 2.32 Ga and 2.12 Ga ages obtained from altered patchy zones or from domains with ghost-like or bleached relic zoning in the zircons are interpreted to date two hydrothermal events that affected the granites. These pulses of hydrothermal activity could be related to the emplacement of the 2.4 Ga Bangalore dyke swarms (e.g. Halls *et al.* 2007; French & Heaman, 2010; Kumar, Hamilton & Halls, 2012) and the 2.17–2.18 Ga Northern Dharwar dykes (French & Heaman, 2010), the equivalents of which have also been reported from around the Cuddapah basin (Demirer, 2012). Furthermore, there are indications of regional-scale metamorphism followed by hydrothermal activity in the EDC at *c.* 2.30–2.37 Ga (Anand *et al.* 2014), also seen in the depleted $^{187}Os/^{186}Os$ of komatiitic amphibolites due to shearing and alteration at *c.* 2.40 Ga (Walker *et al.* 1989), probably associated with the amalgamation of

https://doi.org/10.1017/S0016756817000140 Published online by Cambridge University Press

Table 2. EPMA (wt % oxide) and LA-ICPMS trace element (ppm) analysis of unaltered and altered zircons from the basement granite

	Unaltered zircon								Altered zircon												
	1	2	3	4	5	6	7	8	1	2	3	4	5	6	7	8	9	10	11	12	13
P_2O_5	0.04	0.02	0.11	0.04	0.02	0.00	0.00	0.13	0.00	0.02	0.02	0.02	0.22	0.13	0.20	0.02	0.09	0.56	0.22	0.09	0.07
SiO_2	32.97	32.69	31.38	31.41	31.66	31.98	30.79	30.29	29.35	28.65	25.33	27.36	25.61	29.72	28.77	29.37	28.52	26.63	29.29	27.79	28.45
ZrO_2	63.26	63.35	62.07	64.51	64.97	66.5	67.35	64.57	54.49	55.17	56.65	51.86	51.42	52.55	51.56	47.80	49.83	54.44	57.03	51.69	52.55
Al_2O_3	0.17	0.25	0.32	0.30	0.08	0.00	0.02	0.40	1.40	1.11	1.55	1.10	1.97	1.59	2.02	2.23	1.89	1.10	0.64	1.13	1.23
HfO_2	2.33	2.09	1.83	1.45	1.37	1.38	1.29	1.32	1.25	1.30	1.64	1.11	1.25	1.69	1.87	1.60	1.70	1.53	1.27	1.11	1.41
FeO	0.09	0.06	0.71	0.81	0.36	0.32	0.73	0.36	1.18	0.99	0.64	4.50	0.28	0.64	0.64	1.74	0.59	0.76	0.49	0.55	1.12
CaO	0.22	0.21	1.86	0.43	0.10	0.00	0.01	0.73	1.94	1.80	3.68	1.80	3.09	1.92	2.48	1.58	2.04	1.85	1.15	2.38	1.90
K_2O	0.00	0.00	0.00	0.05	0.00	0.00	0.02	0.05	0.18	0.19	0.04	0.18	0.00	0.00	0.00	0.00	0.00	0.00	0.11	0.18	0.20
PbO	0.01	0.02	0.02	0.03	0.01	0.01	0.03	0.02	0.02	0.03	0.25	0.03	0.05	0.03	0.03	0.02	0.04	0.06	0.03	0.03	0.02
Total	**99.09**	**98.69**	**98.3**	**99.03**	**98.57**	**100.19**	**100.24**	**97.87**	**89.81**	**89.26**	**89.8**	**87.96**	**83.89**	**88.27**	**87.57**	**84.36**	**84.7**	**86.93**	**90.23**	**84.95**	**86.95**
La	2	4	4	2	3	2	3	3	1126	1282	644	1206	403	141	378	415	241	376	231	475	116
Ce	18	29	26	10	22	14	45	15	2823	3251	2076	4196	1298	679	1249	1512	885	1310	881	1504	517
Pr	1	2	2	1	2	1	2	1	472	520	350	694	250	109	209	280	136	184	137	235	77
Nd	5	14	13	5	11	6	12	7	2298	2461	1766	3748	1383	661	1040	1492	686	940	762	1272	424
Sm	5	8	9	4	7	5	9	5	810	1072	519	1431	551	351	448	661	374	436	508	729	320
Eu	2	7	6	2	5	2	6	3	381	506	719	904	236	182	567	439	285	579	332	445	197
Gd	14	22	21	11	21	14	23	15	998	1835	636	1644	614	581	835	1271	692	804	1000	1370	637
Tb	5	6	6	3	6	4	6	5	198	327	110	314	114	108	182	280	166	166	251	319	161
Dy	52	65	63	37	62	43	61	47	1579	2286	882	2346	825	754	1404	2423	1392	1360	1947	2578	1322
Ho	18	21	21	13	20	15	21	17	370	475	226	496	180	167	331	590	327	310	438	556	290
Er	79	91	91	61	88	67	93	75	1240	1369	784	1553	557	543	1059	1880	994	1004	1355	1844	930
Tm	18	21	19	14	18	16	20	17	232	230	144	273	104	100	200	352	193	193	250	331	172
Yb	181	199	198	130	182	156	195	165	1775	1778	1055	1969	825	778	1554	2772	1546	1438	1934	2653	1406
Lu	25	30	30	22	30	25	39	34	234	226	150	265	103	107	209	364	192	186	246	345	171
Y	528	645	533	547	581	523	621	435	9505	11339	6813	12 722	4566	4412	8336	15 756	8586	8458	10 065	14 799	6662
U	298	323	316	302	317	305	305	298	9509	22 328	8925	9793	5227	1844	3822	6178	2515	2131	2938	3738	1828
Th	165	159	161	163	160	163	164	164	8078	159 358	22 280	3740	2134	1612	14 905	7458	1654	1511	3671	2458	1532
Th/U	0.55	0.49	0.51	0.54	0.50	0.53	0.54	0.55	0.85	7.14	2.50	0.38	0.41	0.87	3.90	1.21	0.66	0.71	1.25	0.66	0.84
$(La/Y)_N$	0.03	0.04	0.05	0.03	0.03	0.03	0.03	0.04	0.78	0.75	0.63	0.63	0.58	0.21	0.30	0.17	0.19	0.29	0.15	0.21	0.12

https://doi.org/10.1017/S0016756817000140 Published online by Cambridge University Press

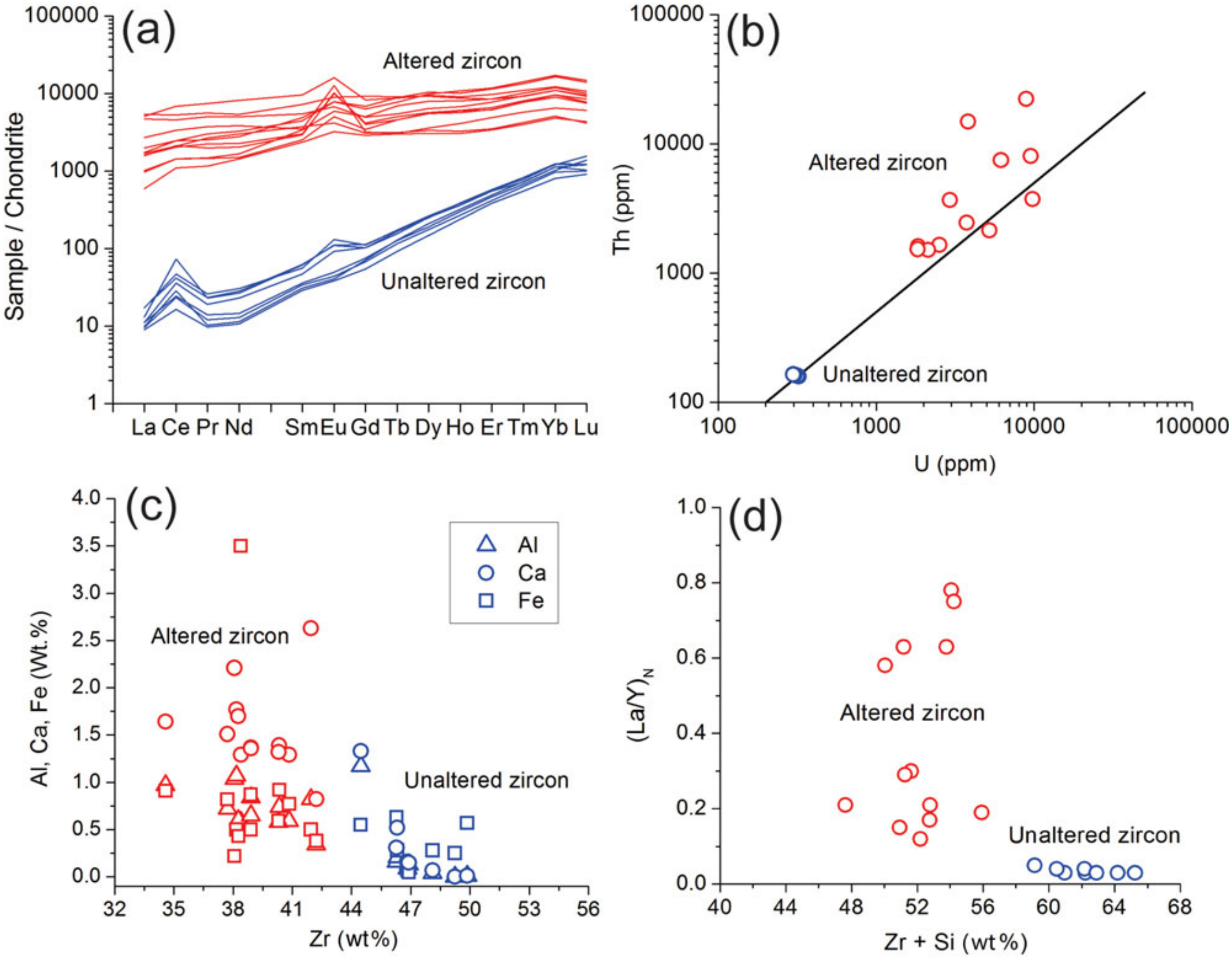

Figure 7. (Colour online) REE and major element characteristics of the hydrothermally altered zircon compared to those of the unaltered zircon.

the eastern and western Dharwar cratons at 2.45–2.39 Ga (Krogstad, Hanson & Rajamani, 1991, 1995). A similar age has also been reported by Hazarika, Pruseth & Mishra (2015), attributed to post-metamorphic shearing and alteration. Ages of 2298 ± 23 Ma and 2373 ± 23 Ma have been reported from altered meta-basalts in the Hutti–Maski greenstone belt, and an age of 2298 ± 22 Ma to 2348 ± 23 Ma in the granitoids to the east of it (A. Schmidt, unpub. Diploma thesis, Univ. Münster, 2003; A. Schmidt *et al.* unpub. abstract, 2004). Accordingly the time span of deposition of the gritty quartzite horizon can be constrained between 2.53 and 2.12 Ga.

The uraninite in the gritty quartzite yielded a wide spectrum of ages (Fig. 5b) that overlap with a major part of the age spectrum furnished by monazite in the granite (Fig. 2a). This again supports the fact that the basement and the quartzite were affected by a common set of hydrothermal episodes. The wide spectrum of ages seen in these two minerals may be linked to the effects of younger magmatic activities from around the Cuddapah region (e.g. at 1788 Ma (U–Pb baddeleyite age with lower intercept at 400 Ma; Demirer, 2012) and 1192 Ma (Pradhan, Pandit & Meert, 2008)) and to tectonothermal events in the neighbouring orogenic belts. Disturbance of isotope systems during younger tectonothermal events is reflected in the wide range of K–Ar (935, 1073, 1280 and 1349 Ma; Mallikarjuna *et al.* 1995) and Ar–Ar ages (1349 Ma (Mallikarjuna *et al.* 1995); 800 and 1200 Ma (Goutham *et al.* 2011)) of the Tirupati/Chitoor dyke swarms to the south of the Cuddapah basin.

In the Palnad sub-basin, the lowermost unit of the Banganapalle Quartzite is the gritty quartzite, which contains coarse lithic as well as feldspathic fragments. We have, for the first time, identified siliceous stromatolites in this quartzite which deceptively look like rounded pebbles (Fig. 4b). This probably led earlier workers to correlate the gritty quartzite in the Palnad sub-basin with the conglomerate underlying the Banganapalle Quartzite in the Kurnool sub-basin. As seen in Figure 1c, the top of the gritty quartzite even in very closely spaced boreholes does not maintain a uniform level when the bounding surfaces of the other units are matched. This indicates differential erosion of the gritty quartzite, with a possible unconformity above it which has evaded detection because of inadequate surface exposures. A similar scenario

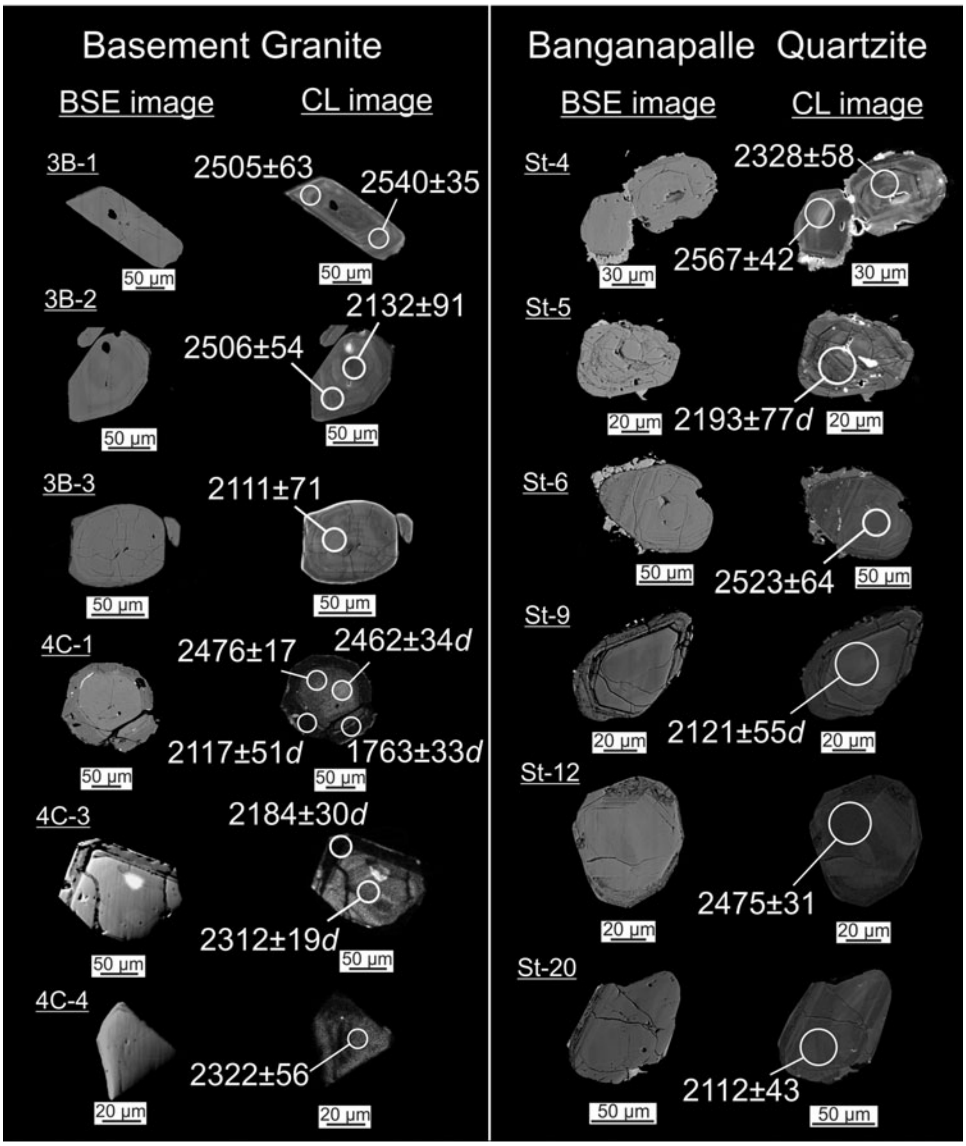

Figure 8. Representative BSE and CL images of zircons from the basement granite and the Banganapalle Quartzite. The LA-ICPMS U–Pb ages for the indicated spots are given. Those with the suffix 'd' are discordant and denote the $^{207}Pb/^{206}Pb$ ages.

exists for the Gandikota Formation, and a disconformity has been proposed between it and the underlying Chitravati Group (Collins *et al.* 2015). Further, the siliceous stromatolites in the gritty quartzite are similar to the *collenia*-type carbonate stromatolites reported from the Vempalle Limestone (Schopf & Prasad, 1978). Thus, the gritty quartzite in the Palnad sub-basin could actually be equivalent to the Gulcheru Quartzite that underlies the Vempalle Limestone in the Papaghni sub-basin, rather than to the conglomerate underlying the Banganapalle Quartzite in the Kurnool sub-basin.

The organic-rich layers in stromatolite-like fragments within the gritty quartzite represent microbial mats those produced the siliceous stromatolites seen in the gritty quartzite. Cell walls of bacteria are generally negatively charged and attract positively charged cations. The water adjacent to the cell walls may locally become supersaturated in some cations, causing them to precipitate as stable complexes even when the ambient conditions may not allow precipitation of these cations (e.g. Newsome, Morris & Lloyd, 2014). The uraninite laminations that alternate with organic-rich layers in the stromatolites thus could be authigenic precipitates on the cell walls of the bacteria forming the microbial mats. Thus, the uraninite ages could in principle closely correspond to the timing of sedimentation. However, microtextural evidence indicates that the uraninite has been extensively remobilized during later hydrothermal alteration of the rocks. The dissolution–reprecipitation and redistribution of uraninite has obliterated the original laminations (Fig. 4c) and remobilized U and Pb, as seen from the occurrence of galena and Pb-oxide associated with the uraninite (Fig. 3g, h). It is also reflected in the large spread in the uraninite age spectrum and the scarcity of older ages. The oldest age of 1989 ± 19 Ma measured from the uraninite is practically indistinguishable from the $^{207}Pb/^{206}Pb$ zircon ages of 1995 ± 11 Ma for A-type granites intrusive into the EDC basement

https://doi.org/10.1017/S0016756817000140 Published online by Cambridge University Press

Table 3. LA-ICPMS U–Pb isotope data and ages of zircon from the Banganapalle Quartzite and the basement granite

			Isotope ratios							Age (Ma)							
Anal. No.	Spot size (μm)	U conc. (ppm)	$^{206}Pb/^{238}U$	±2σ	$^{207}Pb/^{235}U$	±2σ	$^{207}Pb/^{206}Pb$	±2σ	ρ	$^{206}Pb/^{238}U$	±2σ	$^{207}Pb/^{235}U$	±2σ	$^{207}Pb/^{206}U$	±2σ	*f^{206}Pb/ (%)	Conc. (%)
Banganapalle Quartzite																	
St-1	25	10045	0.028	0.003	0.475	0.066	0.1219	0.0084	0.87	179	21	394	46	1985	123	4.58	9
St-2	25	4208	0.045	0.006	0.853	0.130	0.1366	0.0069	0.94	285	40	626	71	2185	88	2.96	13
St-3	25	474	0.481	0.024	10.900	0.640	0.1643	0.0051	0.85	2532	105	2515	55	2501	52	0.42	101
St-3	25	178	0.487	0.023	11.324	0.627	0.1686	0.0048	0.86	2559	100	2550	52	2543	48	0.25	101
St-4	25	312	0.496	0.026	11.700	0.688	0.1709	0.0043	0.90	2598	114	2581	55	2567	42		101
St-4	25	1306	0.427	0.024	8.742	0.569	0.1485	0.0050	0.86	2292	107	2311	59	2328	58	1.06	98
St-5	25	858	0.298	0.023	5.643	0.505	0.1373	0.0061	0.87	1682	115	1923	77	2193	77	0.36	77
St-6	25	674	0.479	0.026	11.010	0.736	0.1665	0.0063	0.82	2525	115	2524	62	2523	64	0.01	100
St-7	25	2276	0.178	0.009	3.242	0.180	0.1324	0.0034	0.89	1054	48	1467	43	2131	45	1.50	49
St-7	25	5261	0.047	0.003	0.732	0.070	0.1127	0.0082	0.65	297	18	558	41	1843	133	5.80	16
St-8	30	207	0.478	0.010	10.937	0.356	0.1661	0.0040	0.68	2517	46	2518	30	2519	40	1.03	100
St-8	25	193	0.459	0.012	10.558	0.466	0.1669	0.0061	0.57	2434	51	2485	41	2527	61	0.42	96
St-9	25	1119	0.105	0.004	1.906	0.089	0.1317	0.0041	0.74	643	21	1083	31	2121	55	1.59	30
St-10	25	101	0.481	0.025	11.233	0.686	0.1694	0.0055	0.85	2531	109	2543	57	2552	54	0.12	99
St-10	25	150	0.324	0.013	7.629	0.425	0.1710	0.0066	0.73	1807	64	2188	50	2567	64	0.08	70
St-11	25	916	0.111	0.009	2.561	0.210	0.1676	0.0043	0.95	678	50	1290	60	2534	43	0.54	27
St-12	25	707	0.481	0.009	10.733	0.280	0.1618	0.0030	0.70	2532	38	2500	24	2475	31	0.06	102
St-13	30	412	0.476	0.007	10.860	0.265	0.1656	0.0033	0.59	2508	30	2511	23	2514	33		100
St-13	30	1806	0.148	0.002	2.765	0.057	0.1357	0.0023	0.58	889	10	1346	15	2173	30	1.77	41
St-14	30	250	0.480	0.016	11.292	0.479	0.1707	0.0044	0.79	2527	70	2548	40	2564	43		99
St-15	30	377	0.487	0.007	11.251	0.241	0.1677	0.0026	0.68	2556	31	2544	20	2535	26		101
St-16	30	284	0.473	0.013	10.715	0.385	0.1644	0.0036	0.80	2495	59	2499	33	2502	37		100
St-17	30	338	0.480	0.008	11.067	0.245	0.1672	0.0024	0.76	2527	35	2529	21	2530	24	0.05	100
St-18	30	576	0.265	0.006	5.946	0.173	0.1630	0.0029	0.79	1513	31	1968	25	2487	30	0.63	61
St-18	25	1151	0.069	0.004	1.392	0.092	0.1454	0.0033	0.94	433	26	886	39	2293	39	2.78	19
St-19	30	137	0.482	0.008	11.137	0.267	0.1677	0.0030	0.68	2535	34	2535	22	2534	30	0.01	100
St-19	30	226	0.481	0.008	11.166	0.278	0.1683	0.0032	0.64	2532	33	2537	23	2541	32	0.69	100
St-20	30	846	0.389	0.009	7.021	0.238	0.1310	0.0032	0.69	2116	42	2114	30	2112	43	0.76	100
St-21	30	1265	0.480	0.008	11.124	0.243	0.1680	0.0025	0.72	2528	33	2534	20	2538	25	1.47	100
St-21	30	1219	0.082	0.006	1.784	0.133	0.1570	0.0032	0.96	511	35	1040	49	2423	35	1.71	21
St-22	30	2835	0.088	0.002	1.420	0.040	0.1174	0.0021	0.78	542	12	897	17	1918	32	0.16	28
St-22	30	1606	0.273	0.004	5.057	0.139	0.1345	0.0031	0.56	1554	21	1829	23	2158	40	0.12	72
St-23	30	769	0.236	0.003	5.192	0.101	0.1596	0.0024	0.65	1366	16	1851	17	2451	25	0.12	56
Basement granite																	
2B-1	25	278	0.494	0.020	11.481	0.713	0.1686	0.0080	0.64	2587	85	2563	58	2544	80	2.38	102
2B-2	25	373	0.485	0.019	11.081	0.513	0.1658	0.0042	0.84	2548	81	2530	43	2516	43	3.33	101
2B-2	25	598	0.489	0.020	11.485	0.526	0.1702	0.0034	0.90	2568	88	2563	43	2560	33	0.43	100
3B-1	25	173	0.489	0.021	11.350	0.548	0.1682	0.0035	0.90	2568	92	2552	45	2540	35	0.31	101
3B-1	25	362	0.476	0.026	10.808	0.708	0.1647	0.0062	0.82	2509	112	2507	61	2505	63	1.49	100
3B-2	25	1612	0.398	0.017	7.272	0.491	0.1325	0.0069	0.64	2160	80	2145	60	2132	91	4.02	101
3B-2	25	1087	0.477	0.023	10.849	0.622	0.1648	0.0053	0.83	2516	99	2510	53	2506	54	0.07	100
3B-3	25	3407	0.388	0.016	7.004	0.401	0.1310	0.0053	0.71	2113	73	2112	51	2111	71	0.12	100
3B-4	25	7808	0.070	0.004	0.905	0.053	0.0936	0.0030	0.85	437	21	654	28	1500	60	0.12	29
3B-4	25	5000	0.071	0.003	1.048	0.056	0.1074	0.0026	0.90	441	20	728	28	1756	44	0.10	25
4C-1	25	355	0.328	0.019	7.270	0.448	0.1606	0.0032	0.94	1830	93	2145	55	2462	34	0.02	74
4C-1	25	2012	0.141	0.008	2.560	0.161	0.1315	0.0038	0.89	852	45	1289	46	2117	51	0.12	40
4C-1	25	468	0.359	0.021	8.018	0.479	0.1619	0.0016	0.99	1978	100	2233	54	2476	17	0.11	80
4C-1	25	9845	0.048	0.003	0.720	0.041	0.1078	0.0020	0.95	305	16	551	24	1763	33	3.40	17
4C-2	25	5135	0.082	0.007	1.568	0.142	0.1387	0.0027	0.98	508	43	958	56	2211	34	5.03	23
4C-3	25	538	0.280	0.015	5.672	0.314	0.1471	0.0016	0.98	1590	76	1927	48	2312	19	1.19	69
4C-3	25	1462	0.057	0.004	1.077	0.072	0.1366	0.0024	0.97	359	22	742	35	2184	30	1.42	16
4C-4	25	2749	0.106	0.006	1.830	0.108	0.1249	0.0034	0.89	651	32	1056	39	2028	48	1.78	32
4C-4	25	578	0.441	0.022	8.990	0.532	0.1479	0.0048	0.84	2355	98	2337	54	2322	56	0.07	101

*Percentage of common ^{206}Pb

near Srikalahasti reported by Vadlamani *et al.* (2014). Those authors link the granite emplacement to the initiation of the Cuddapah basin. However, the uraninite mineralization obviously has to be younger than the gritty quartzite that might have been deposited after the opening of the Cuddapah basin before 2.12 Ga, the age furnished by the hydrothermal zircons supporting at least an early Palaeoproterozoic age for the deposition of the gritty quartzite. Collins *et al.* (2015) have reached a similar conclusion from their data on detrital zircon ages. They obtained a discordia upper intercept age of 1924 ± 25 Ma from the zircons in the Pullivendla Quartzite and considered it to be the maximum age of deposition of the Chitravati Group. If so, the sediments of the underlying Papaghni Group of the lower Cuddapah Supergroup must have been deposited before 1.92 Ga. The youngest detrital zircon age reported by them from the Gulcheru Quartzite is 2490 ± 19 Ma, which constrains the deposition of the earliest Cuddapah sediments (i.e. Gulcheru Quartzite

https://doi.org/10.1017/S0016756817000140 Published online by Cambridge University Press

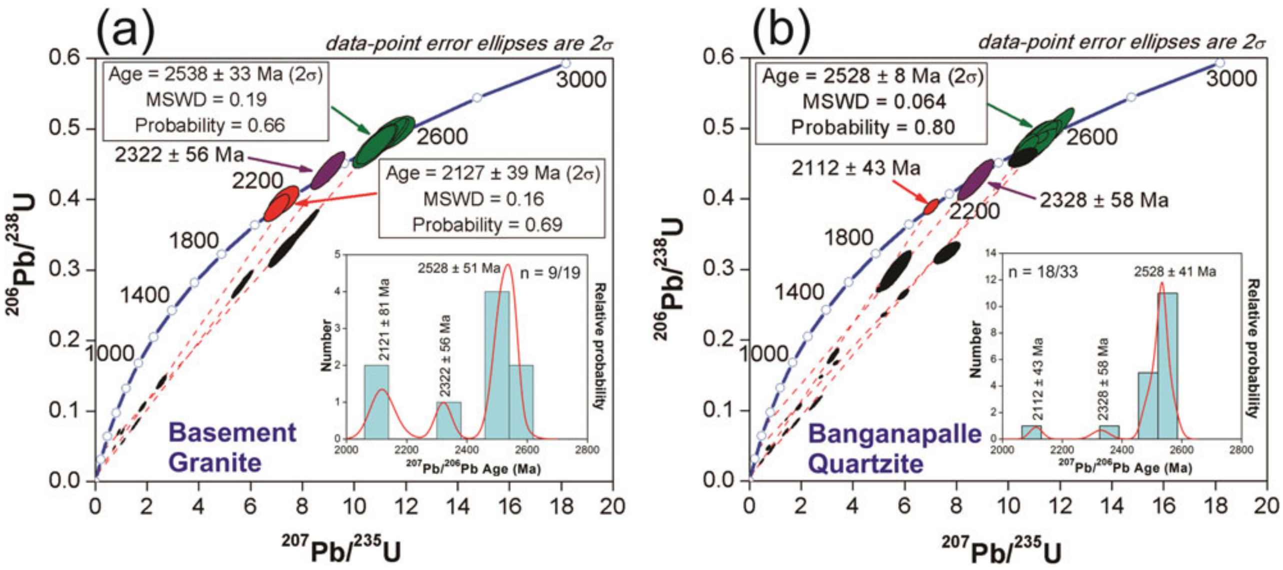

Figure 9. (Colour online) Concordia diagrams for the zircons from (a) basement granite; (b) Banganapalle Quartzite. Corresponding probability density plots of ≥90 % concordant ages are provided in the insets. Error ellipses are at the 2 standard deviations level. The discordias indicate the latest Pb-loss event at ~90 Ma in both the basement and the quartzite.

and its equivalents) between 2.49 and 1.92 Ga. The maximum age of the gritty quartzite and the Gulcheru Quartzite, and therefore that of the opening of the Cuddapah basin, still remains open-ended and with our new zircon age data can be constrained to a narrower interval of 2.53–2.12 Ga.

5.b. The age of the Kurnool Group

The Kurnool and Palnad sub-basins are considered to be stratigraphically equivalent, and have traditionally been correlated with the Vindhyan and the Chhattisgarh basins (Medlicott & Blanford, 1879; Raha, 1987; Chaudhuri *et al.* 2002), which were earlier assigned a Neoproterozoic age based on Ediacaran-like fossils found in the Vindhyan (Azmi, 1998; De, 2003, 2006; Azmi *et al.* 2006, 2008; Joshi, Azmi & Srivastava, 2006; Kumar & Pandey, 2008). However, recent age data show that the oldest sediments in the Vindhyan basin are Palaeo- to Mesoproterozoic in age (e.g. 1721–1600 Ma (Rasmussen *et al.* 2002; Ray *et al.* 2002; Ray, Veizer & Davis, 2003; Sarangi, Gopalan & Kumar, 2004; Bengtson *et al.* 2009)) and that the basin closed at ~900 Ma (Gopalan *et al.* 2013). Similarly, sedimentation in the Chhattisgarh basin spanned from ~1400 Ma (Bickford *et al.* 2011) to ~1007 Ma (Patranabis-Deb *et al.* 2007). Thus, the emerging geochronological evidence strongly suggests that the sediments of the Vindhyan and the Chhattisgarh basins may have been deposited during the Palaeo- and Mesoproterozoic and this may also be applicable to the Kurnool Group. This contradicts the Neoproterozoic age assigned to the rocks of the Kurnool Group on the basis of the presence of Ediacaran fossils. Sharma & Shukla (2012) have reported helically coiled Ediacaran *Obruchevella* species. However, *Obruchevella* has been reported from Neoproterozoic as well as Palaeozoic rocks (Mankiewicz, 1992), and in the absence of robust isotopic age constraints this interpretation based only on the fossil record is questionable, as has been exemplified by the discordance between the isotopic and biostratigraphic ages for the Vindhyan sediments (Bengtson *et al.* 2009). Sedimentary carbonate xenoliths apparently belonging to the Bhima/Kurnool basin (A. Dongre *et al.* unpub. abstract, 2007; Dongre, Chalapathi Rao & Kamde,2008; Chalapathi Rao *et al.* 2010) in the Siddanpalli and Raichur kimberlites, which intruded the EDC at ~1090 Ma (Kumar, Heaman & Manikeyamba, 2007), imply that the Kurnool Group rocks may not be younger than the Mesoproterozoic. The diamonds from the base of the Banganapalle Quartzite could have been derived from kimberlites or from lamproites. The Wajrakarur kimberlites are the potential sources of these diamonds (Krishnan, 1964; Nagaraja Rao *et al.* 1987; Chaudhuri *et al.* 1999), which have been dated at 1140–1105 Ma (Ar–Ar phlogopite age: Crawford & Compston, 1973; Osborne *et al.* 2011). If true, this will indicate a post-Mesoproterozoic age for the Kurnool sediments, in agreement with the inference by Sharma & Shukla (2012), but in contradiction to Dongre, Chalapathi Rao & Kamde (2008) who advocate at least a Midproterozoic age. Other kimberlites could also be the source of the diamonds. However, all the known kimberlites in the area have late Mesoproterozoic ages (Kumar *et al.* 1993, 2001; Chalapathi Rao *et al.* 1996, 1999, 2013; Kumar, Heaman & Manikeyamba, 2007; Babu *et al.* 2008), so if the occurrence of diamond in the Banganapalle Quartzite and that of sedimentary carbonate xenoliths in the kimberlites are to be reconciled with this, then the source of diamonds will apparently be the lamproites. Chalapathi Rao *et al.* (2010) suggested lamproitic rocks analogous to the ~1417 Ma Chelima lamproites (Chalapathi Rao *et al.* 1999) as the source

https://doi.org/10.1017/S0016756817000140 Published online by Cambridge University Press

of the diamonds in the Banganapalle Quartzite. Joy *et al.* (2012) reached a similar conclusion on the basis of the dissimilarity in the composition of garnets from the conglomerate at the base of the Banganapalle Quartzite vis-à-vis those in the Wajrakarur kimberlites. In contrast, Collins *et al.* (2015), on the basis of detrital zircon characteristics, support a westward provenance for the Papaghni as well as the Kurnool sediments, suggesting that the diamonds most likely were derived from the Wajrakarur and the Narayanpet kimberlite fields.

Bickford *et al.* (2013) obtained zircon ages of 2522 ± 36 Ma from the purported felsic tuff bed (Saha & Tripathy, 2012) within the Owk Shale overlying the Banganapalle Quartzite. Only two grains yielded ages of 1880 and 3292 Ma. The 1.88 Ga age is similar to the age of baddeleyite from a mafic sill near the base of the Cuddapah basin (French *et al.* 2008). Collins *et al.* (2015) have presented stratigraphically constrained zircon U–Pb ages from over the entire Cuddapah basin. For the Banganapalle Quartzite, the youngest age reported by those authors is 2516 ± 16 Ma. In the Paniam Quartzite that overlies the Owk Shale, they obtained a single near-concordant zircon age of 913 ± 11 Ma, the next youngest age being 1717 ± 20 Ma. The new age data lead to the possibility that the Paniam Quartzite was deposited after 913 ± 11 Ma, which is also consistent with the post-Mesoproterozoic age implied by diamond occurrence in the Banganapalle Quartzite.

The sediments in the Kurnool sub-basin were probably deposited later in the Mesoproterozoic, most likely after the emplacement of the kimberlites of the EDC at *c.* 1100 Ma (Kumar *et al.* 1993, 2001; Chalapathi Rao *et al.* 1996, 1999, 2013; Kumar, Heaman & Manikeyamba, 2007; Babu *et al.* 2008), consistent with diamond occurrence in the Banganapalle Quartzite in the Kurnool sub-basin as well as with the report of Ediacaran fossils in the Owk Shale (Sharma & Shukla, 2012).

5.c. The cessation of sedimentation in the Kurnool sub-basin

The final closure of the Kurnool sub-basin, and thus the total span of sedimentation in the Kurnool sub-basin, still remains unresolved. According to recently published Pb-isotope data (Gopalan *et al.* 2013), sedimentation in the Vindhyan basin ceased at *c.* 900 Ma. This age is similar to the timing of the closure of the Chhattisgarh basin (~1007 Ma; Patranabis-Deb *et al.* 2007). The interpretation by A. Dongre *et al.* (unpub. abstract, 2007), Dongre, Chalapathi Rao & Kamde (2008) and Chalapathi Rao *et al.* (2010) that the Kurnool sediments are older than 1090 Ma is thus in agreement with these ages, but inconsistent with the occurrence of 913 ± 11 Ma detrital zircon in the Paniam Quartzite (Collins *et al.* 2015). The 913 Ma detrital zircon does not strictly contradict the observation of Gopalan *et al.* (2013) implying almost simultaneous closure of all the Proterozoic basins of India. However, it does not necessarily imply that the age of the Kurnool sediments cannot be <900 Ma. Thus the Paniam Quartzite may even be much younger, if the Owk Shale is truly Ediacaran in age (Sharma & Shukla, 2012). Very young ages recorded by uraninite in the gritty quartzite, consistent with the resetting of zircon ages at ~90 Ma, indicate *in situ* modification of the age record and thus are incapable of putting a constraint on either the beginning or the cessation of sedimentation of the Kurnool sediments.

6. Conclusions

In the Koppunuru area the basal gritty quartzite apparently belonging to the Banganapalle Quartzite in the Palnad sub-basin and the basement granite have been witnesses to several episodes of hydrothermal activity that have left their imprints on the isotope systematics of zircon, monazite and uraninite. Thus the younger ages furnished by zircon are probably due to *in situ* hydrothermal resetting of their isotopic clocks and should be linked to the sediment depositional events only with caution. In the Palnad sub-basin, the basal gritty quartzite is equivalent in age to the Gulcheru Quartzite. Thus the earliest sedimentation in the Palnad sub-basin was contemporaneous with the beginning of sedimentation elsewhere in the Cuddapah basin and can be constrained between 2.53 and 2.12 Ga. The Kurnool sediments most likely were deposited after 1100 Ma, signifying the presence of an unconformity above the gritty quartzite. The carbonate xenoliths in the Siddanpalli and Raichur kimberlites (A. Dongre *et al.* unpub. abstract, 2007) are likely to have been derived from rocks belonging to the equivalents of the Vempalle Limestone.

Acknowledgements. This work was supported by a BRNS (Board of Research in Nuclear Sciences) research grant (2011/36/60-BRNS/809) from DAE (Department of Atomic Energy) India to K.L.P. and D.C.P. D.S. thanks the UGC, New Delhi, for financial assistance received in the form of a research fellowship. SEM-BSE imaging and EPMA data were generated by the equipment procured through a DST (Department of Science and Technology) funding (IR/S4/ESF-08/2005) to the Department of Geology and Geophysics, IIT Kharagpur. The LA-ICPMS facility was funded through Diamond Jubilee Grants of IIT Kharagpur and is gratefully acknowledged.

Supplementary material

To view supplementary material for this article, please visit https://doi.org/10.1017/S0016756817000140.

References

Anand, R., Balakrishnan, S., Kooijman, E. & Mezger, K. 2014. Neoarchean crustal growth by accretionary processes: evidence from combined zircon-titanite U-Pb isotope studies on granitoid rocks around the

Hutti greenstone belt, Eastern Dharwar Craton, India. *Journal of Asian Earth Science* **79**, 72–85.

AZMI, R. J. 1998. Discovery of Lower Cambrian small shelly fossils and brachiopods from the Lower Vindhyan of Son Valley, Central India. *Journal of the Geological Society of India* **52**, 381–9.

AZMI, R. J., JOSHI, D., TEWARI, B. N., JOSHI, M. N., MOHAN, K. & SRIVASTAVA, S. S. 2006. Age of the Vindhyan Supergroup of Central India: an exposition of biochronology vs radiochronology. In *Micropaleontology: Application in Stratigraphy and Paleoceanography* (ed. D. K. Sinha), pp. 29–62. New Delhi: Narosa Publishing House

AZMI, R. J., JOSHI, D., TIWARI, B. N., JOSHI, M. N. & SRIVASTAVA, S. S. 2008. A synoptic view on the current discordant geo-and biochronological ages of the Vindhyan Supergroup, central India. *Himalayan Geology* **29**, 177–91.

BABU, E. V. S. S. K., GRIFFIN, W. L., MUKHERJEE, A., O'REILLY, S. Y. & BELOUSOVA, E. A. 2008. Combined U–Pb and Lu–Hf analysis of megacrystic zircons from the Kalyandurg-4 kimberlite pipe, S. India: implications for the emplacement age and Hf isotopic composition of the cratonic mantle. 9th International Kimberlite Conference Extended Abstract No. 9IKC-A-00142

BENGTSON, S., BELIVANOVA, V., RASUMUSSEN, B. & WHITEHOUSE, M. 2009. The controversial "Cambrian" fossils of the Vindhyan are real but more than a billion years older. *Proceedings of the National Academy of Sciences of the United States of America* **106**(19), 7729–34.

BICKFORD, M. E., BASU, A., PATRANABIS-DEB, S., DHANG, P. C. & SCHIBER, J. 2011. Depositional history of the Chhattisgarh basin, central India: constraints from new SHRIMP zircon ages. *Journal of Geology* **119**, 33–50.

BICKFORD, M. E., SAHA, D., SCHIEBER, J., KAMENOV, G., RUSSELL, A. & BASU, A. 2013. New U-Pb ages of zircons in the Owk Shale (Kurnool Group) with reflections on Proterozoic porcellanites in India. *Journal of the Geological Society of India* **82**, 207–16.

CHAKRABORTY, P. P., DAS, P., SAHA, S., DAS, K. R., MISHRA, S. & PAUL, P. 2012. Microbial mat related structures (MRS) from Mesoproterozoic Chhatisgarh and Khariar basins, Central India and their bearing on shallow marine sedimentation. *Episodes* **35**, 513–23.

CHALAPATHI RAO, N. V., DONGRE, A. N., KAMDE, G., SRIVASTAVA, R. K., SRIDHAR, M. & KAMINSKY, F. E. 2010. Petrology, geochemistry and genesis of newly discovered Mesoproterozoic highly magnesian, calcite-rich kimberlites from Siddanpalli, Eastern Dharwar Craton, Southern India: products of subduction-related magmatic sources? *Mineralogy and Petrology* **98**, 313–28.

CHALAPATHI RAO, N. V., MILLER, J. A., GIBSON, S. A., PYLE, D. M. & MADHAVAN, V. 1999. Precise $^{40}Ar/^{39}Ar$ dating of Kotakonda kimberlite and Chelima lamproite, India: implication to the timing of mafic dyke swarm activity in the Eastern Dhawar craton. *Journal of the Geological Society of India* **53**, 425–32.

CHALAPATHI RAO, N. V., MILLER, J. A., PYLE, D. M. & MADHAVAN, V. 1996. New Proterozoic K-Ar ages for some kimberlites and lamproites from the Cuddapah Basin and Dharwar Craton, south India: evidence for non-contemporaneous emplacement. *Precambrian Research* **79**, 363–9.

CHALAPATHI RAO, N. V., WU, F.-Y., MITCHELL, R. H., LI, Q.-L. & LEHMANN, B. 2013. Mesoproterozoic U–Pb ages, trace element and Sr–Nd isotopic composition of perovskite from kimberlites of the Eastern Dharwar craton, southern India: distinct mantle sources and a widespread 1.1 Ga tectonomagmatic event. *Chemical Geology* **353**, 48–64.

CHAUDHURI, A. K., MUKHOPADHYAY, J., PATRANABIS DEB, S. & CHANDA, S. K. 1999. The Neoproterozoic cratonic successions of peninsular India. *Gondwana Research* **2**, 213–25.

CHAUDHURI, A. K., SAHA, D., DEB, G. K., DEB, S. P., MUKHERJEE, M. K. & GHOSH, G. 2002. The Purana basins of southern cratonic province of India – a case for Mesoproterozoic fossil rifts. *Gondwana Research* **5**, 23–33.

COLLINS, A. S., PATRANABIS-DEB, S., ALEXANDER, E., BERTRAM, C. N., FALSTER, G. M., GORE, R. J., MACKINTOSH, J., DHANG, P. C., SAHA, D., PAYNE, J. L., JOURDAN, F., BACKÉ, G., HALVERSON, G. P. & WADE, B. P. 2015. Detrital mineral age, radiogenic isotopic stratigraphy and tectonic significance of the Cuddapah Basin, India. *Gondwana Research* **28**, 1294–309.

CRAWFORD, A. R. & COMPSTON, W. 1973. The age of the Cuddapah and Kurnool systems, Southern India. *Journal of the Geological Society of Australia* **19**, 453–64.

DE, C. 2003. Possible organisms similar to Ediacaran forms from the Bhander Group, Vindhyan Supergroup, Late Neoproterozoic of India. *Journal of Asian Earth Science* **21**, 387–95.

DE, C. 2006. Ediacara fossil assemblage in the upper Vindhyans of Central India and its significance. *Journal of Asian Earth Science* **27**, 660–86.

DEMIRER, K. 2012. *U-Pb baddeleyite ages from mafic dyke swarms in Dharwar craton, India – links to an ancient supercontinent*. Master's thesis, Lund University, Lund, Sweden. Published thesis.

DONGRE, A., CHALAPATHI RAO, N. V. & KAMDE, G. 2008. Limestone xenolith in Siddanpalli kimberlite, Gadwal granite-greenstone terrain, Eastern Dharwar craton, Southern India: remnant of Proterozoic Platformal cover sequence of Bhima/Kurnool age? *Journal of Geology* **116**, 184–91.

FRENCH, J. E. & HEAMAN, L. M. 2010. Precise U-Pb dating of Proterozoic mafic dyke swarms of the Dharwar craton, India: implications for the existence of the Neoproterozoic supercraton Sclavia. *Precambrian Research* **183**, 416–41.

FRENCH, J. E., HEAMAN, L. M., CHACKO, T. & SRIVASTAVA, R. K. 2008. 1891–1883 Ma Southern Bastar-Cuddapah mafic igneous events, India: a newly recognized large igneous province. *Precambrian Research* **160**, 308–22.

GEISLER, T., SCHALTEGGER, U. & TOMASCHEK, F. 2007. Re-equilibration of zircon in aqueous fluids and melts. *Elements* **3**, 43–50.

GOPALAN, K., KUMAR, A., KUMAR, S. & VIJAYAGOPAL, B. 2013. Depositional history of the Upper Vindhyan succession, central India: time constraints from Pb-Pb isochron ages of its carbonate components. *Precambrian Research* **233**, 108–17.

GOUTHAM, M. R., SUBBARAO, K. V., PRASAD, C. V. R. K., PIPER, J. D. A. & MIGGINS, D. P. 2011. Proterozoic mafic dykes from the southern margin of the Cuddapah Basin, India: Part 2 – Paleomagnetism and Ar-Ar geochronology. In *Dyke Swarms: Keys for Geodynamic Interpretation* (ed. R. K. Srivastava), pp. 73–93.

HALLS, H. C., KUMAR, A., SRINIVASAN, R. & HAMILTON, M. A. 2007. Paleomagnetism and U-Pb geochronology of easterly dykes in the Dharwar Craton, India: feldspar clouding, radiating dyke swarms and the position of India at 2.37 Ga. *Precambrian Research* **155**, 47–68.

Harley, S. L., Kelly, N. M. & Möller, A. 2007. Zircon behaviour and the thermal histories of mountain chains. *Elements* **3**, 25–30.

Hazarika, P., Pruseth, K. L. & Mishra, B. 2015. Neoarchean greenstone metamorphism in the Eastern Dharwar Craton, India: constraints from monazite U-Th-Pb_{total} ages and PT pseudosection calculations. *Journal of Geology* **123**, 429–61.

Hoskin, P. W. O. & Schaltegger, U. 2003. The composition of zircon and igneous and metamorphic petrogenesis. *Reviews in Mineralogy and Geochemistry* **53**, 27–62.

Jackson, S. E., Pearson, N. J., Griffin, W. L. & Belousova, E. A. 2004. The application of laser ablation–inductively coupled plasma–mass spectrometry (LA-ICP-MS) to in situ U–Pb zircon geochronology. *Chemical Geology* **211**, 47–69.

Jeyagopal, A. V., Deshpande, M. S. M., Gupta, S., Ramesh Babu, P. V., Umamaheswar, K. & Maithani, P. B. 2011. Uranium mineralization and association of carbonaceous matter in Koppunuru Area, Palnad sub-basin, Cuddapah basin, Andhra Pradesh. *Indian Mineralogist* **45**, 100–11.

Joshi, D., Azmi, R. J. & Srivastava, S. S. 2006. Earliest Cambrian calcareous skeletal algae from Tirohan Dolomite, Chitrakoot, Central India: a new age constraint for the Lower Vindhyan. *Gondwana Geological Magazine* **21**, 73–82.

Joy, S., Jelsma, H. A., Preston, R. F. & Kota, S. 2012. Geology and diamond provenance of the Proterozoic Banganapalle conglomerates, Kurnool Group, India. In *Palaeoproterozoic of India* (eds R. Mazumder & D. Saha), pp. 197–218. Geological Society of London, Special Publication no. 352.

King, W. 1872. *The Kudapah and Kurmul Formations in the Madras Presidency*. Memoir of the Geological Survey of India, Calcutta **8**(Pt I), 346 pp.

Krishnan, M. S. 1964. The Upper Proterozoic of South India. *Journal of the Indian Geological Science Association* **4**, 1–2.

Krogstad, E. J., Hanson, G. N. & Rajamani, V. 1991. U-Pb ages of zircon and sphene for two gneiss terranes adjacent to the Kolar Schist Belt, South India: evidence for separate crustal evolution histories. *Journal of Geology* **99**, 801–16.

Krogstad, E. J., Hanson, G. N. & Rajamani, V. 1995. Sources of continental magmatism adjacent to the late Archean Kolar Suture zone, South India: distinct isotopic and elemental signature of two late Archean magmatic series. *Contributions to Mineralogy and Petrology* **122**, 159–73.

Kumar, A., Gopalan, K., Rao, K. R. P. & Nayak, S. S. 2001. Rb-Sr age of kimberlites and lamproites from Eastern Dharwar Craton, South India. *Journal of the Geological Society of India* **58**, 135–41.

Kumar, A., Hamilton, M. A. & Halls, H. C. 2012. A Paleoproterozoic giant radiating dyke swarm in the Dharwar Craton, southern India. *Geochemistry, Geophysics, Geosystems* **13**, Q02011. doi:10.1029/2011GC003926.

Kumar, A., Heaman, L. M. & Manikeyamba, C. 2007. Mesoproterozoic kimberlites in south India: a possible link to ∼1.1 Ga global magmatism. *Precambrian Research* **154**, 192–204.

Kumar, A., Padma Kumari, V. M., Dayal, A. M., Murthy, D. S. N. & Gopalan, K. 1993. Rb-Sr ages for Proterozoic kimberlites of India: evidence for contemporaneous emplacement. *Precambrian Research* **62**, 227–37.

Kumar, S. & Pandey, S. K. 2008. Arumberia and associated fossils from the Neoproterozoic Maihar Sandstone, Vindhyan Supergroup, Central India. *Journal of the Palaeontological Society of India* **53**, 83–97.

Lakshminarayana, G., Bhattacharjee, S. & Ramanaidu, K. V. 2001. Sedimentation and stratigraphic framework in the Cuddapah basin. *Geological Survey of India Special Publication* **55**, pp. 31–58.

Ludwig, K. R. 2003. *User's Manual for Isoplot 3.00, a Geochronological Toolkit for Microsoft Excel-4*. Berkeley, CA: Berkeley Geochronology Center.

Mallikarjuna, R. J., Bhattacharji, S., Rao, M. N. & Hermes, O. D. 1995. ^{40}Ar-^{39}Ar ages and geochemical characteristics of dolerite dykes around the Proterozoic Cuddapah Basin, South India. *Memoirs of the Geological Society of India* **33**, 307–28.

Mankiewicz, C. 1992. *Obruchevella* and other microfossils in the Burgess Shale: preservation and affinity. *Journal of Paleontology* **66**, 717–29.

Medlicott, H. B. & Blanford, W. T. 1879. *A Manual of the Geology of India. Pt. I and II*. Calcutta: Government of India.

Meijerink, A. M. J., Rao, D. P. & Rupke, J. 1984. Stratigraphic and structural development of the Precambrian Cuddapah basin, SE India. *Precambrian Research* **26**, 57–104.

Nagaraja Rao, B. K., Rajurkar, S. T., Ramalingaswamy, G. & Ravindra Babu, B. 1987. Stratigraphy, structure and evolution of the Cuddapah Basin. *Journal of the Geological Society of India* **6**, 33–86.

Narayanswami, S. 1966. Tectonics of the Cuddapah basin. *Journal of the Geological Society of India* **7**, 33–50.

Newsome, L., Morris, K. & Lloyd, J. R. 2014. The biogeochemistry and bioremediation of uranium and other priority radionuclides. *Chemical Geology* **363**, 164–84.

Osborne, I., Sherlock, S., Anand, M. & Argles, T. 2011. New Ar-Ar ages of southern Indian kimberlites and a lamproite and their geochemical evolution. *Precambrian Research* **189**, 91–103.

Patranabis-Deb, S., Bickford, M. E., Hill, B., Chaudhuri, A. K. & Basu, A. 2007. SHRIMP ages of zircon in the uppermost tuff in Chhattisgarh Basin in central India require up to 500 Ma adjustment in Indian Proterozoic stratigraphy. *Journal of Geology* **115**, 407–15.

Pradhan, V. R., Pandit, M. K. & Meert, J. G. 2008. A cautionary note on the age of the paleomagnetic pole obtained from the Harohalli dyke warms, Dharwar craton, southern India. In *Indian Dykes* (eds R. K. Srivastava, C. Sivaji & N. V. Chalapathi Rao), pp. 339–52. New Delhi: Narosa Publishing House.

Prasad, B. R. & Rao, V. V. 2006. Deep seismic reflection study over the Vindhyans of Rajasthan: implications for geophysical setting of the basin. *Journal of Earth System Science* **115**, 135–47.

Raha, P. K. 1987. Stromatolites and correlation of the Purana (middle to late Proterozoic) basins of peninsular India. In *Purana Basins of Peninsular India* (ed. B. P. Radhakrishna), pp. 393–7. Memoirs of the Geological Society of India no. 6.

Rasmussen, B., Bose, P. K., Sarkar, S., Banerjee, S., Fletcher, I. R. & McNaughton, N. J. 2002. 1.6 Ga U-Pb zircon age for the Chorhat Sandstone, Lower Vindhyan, India: possible implications for early evolution of animals. *Geology* **30**, 103–6.

Ray, J. S., Martin, M. W., Veizer, J. & Bowring, S. A. 2002. U-Pb zircon dating and Sr isotopic systematics of the Vindhyan Supergroup, India. *Geology* **3**, 131–4.

Ray, J. S., Veizer, J. & Davis, W. J. 2003. C, O, Sr and Pb isotope systematics of carbonate sequences of the Vindhyan Supergroup, India: age, diagenesis, correlations and implications for global events. *Precambrian Research* **121**, 103–21.

Saha, D. & Chakraborty, S. 2003. Deformation pattern in the Kurnool and Nallamalai Groups in the northeastern part (Palnad area) of the Cuddapah basin, south India and its implication on Rodinia/Gondwana tectonics. *Gondwana Research* **6**, 573–83.

Saha, D., Chakraborti, S. & Tripathy, V. 2010. Intracontinental thrusts and inclined transpression along eastern margin of the East Dharwar craton, India. *Journal of the Geological Society of India* **75**, 323–37.

Saha, D. & Tripathy, V. 2012. Tuff beds in Kurnool subbasin, southern India and implications for felsic volcanism in Proterozoic intracratonic basins. *Geoscience Frontiers* **3**, 429–44.

Sarangi, S., Gopalan, K. & Kumar, S. 2004. Pb-Pb age of the earliest megascopic, eukaryotic alga bearing Rohtas Formation, Vindhyan Supergroup, India: implications for Precambrian atmospheric oxygen evolution. *Precambrian Research* **121**, 107–21.

Schopf, J. W. & Prasad, K. N. 1978. Microfossils in Collenia-like stromatolites from the Proterozoic Vempalle formation of the Cuddapah Basin, India. *Precambrian Research* **6**, 347–66.

Sharma, M. & Shukla, Y. 2012. Occurrence of helically coiled microfossil obruchevella in the Owk Shale of the Kurnool Group and its significance. *Journal of Earth System Science* **3**, 755–68.

Tripathy, V. & Saha, D. 2013. Plate margin paleostress variations and intracontinental deformations in the evolution of the Cuddapah basin through Proterozoic. *Precambrian Research* **235**, 107–30.

Vadlamani, R., Hashmi, S., Chatterjee, C., Ji, W.-Q. & Wu, F.-Y. 2014. Initiation of the intra-cratonic Cuddapah basin: evidence from Paleoproterozoic (1995 Ma) anorogenic porphyritic granite in Eastern Dharwar Craton basement. *Journal of Asian Earth Sciences* **79**, 235–45.

Walker, R. J., Shirey, S. B., Hanson, G. N., Rajamani, V. & Horan, M. F. 1989. Re-Os, Rb-Sr and O isotopic systematics of the Archean Kolar schist belt, Karnataka, India. *Geochimica et Cosmochimica Acta* **53**, 3005–13.

Wiedenbeck, M., Alle, P., Corfu, F., Griffin, W. L., Meier, M., Oberli, F., Von Quart, A., Roddick, J. C. & Spiegel, W. 1995. Three natural zircon standards for U-Th-Pb, Lu-Th, trace element and REE analysis. *Geostandards Newsletter* **19**, 1–23.